Study of Three Dimensional Casson-Nanofluid Flow due to a Linear Porous Stretching Sheet in the Presence of Double Diffusion Effects

D. R. Kirubaharan[1], A. D. Subhashini[1], G. Murali[2*]

[1]*Department of Mathematics, PRIST University, Thanjavur, India;*

[2]*Department of Mathematics, Geethanjali College of Engineering and technology, Cheeryal, India.*

Abstract: In this work, the bidirectional flow of magnetohydrodynamics (MHD) with slip effects, a magnetic field, and the inclusion of Casson and nanofluid particles is investigated. A stretched sheet that is porous and linear in three dimensions creates this flow. Similarity transformations are used to translate the fundamental boundary layer model into a system of ordinary differential equations. After that, the equations are solved using the Runge-Kutta technique along with shooting technique. The investigation looks at how several parameters, including temperature, concentration, and main and secondary velocities, affect how flow variables change over time. Additionally, it looks at the impact of engineering parameters including mass transfer coefficients, skin-friction coefficients, and heat transfer rates. A combination of tabular and graphical displays is used in this investigation. In the end, the validity of the present model is confirmed by contrasting the numerical values derived from the findings that have been published with the available data. This instruction give you guidelines for preparing papers for ASSA publication. Please use this document as a template to prepare your manuscript for submission.

Keywords: Multiple slip effects; MHD; Three dimensional; Nanofluid; Casson fluid; Porous medium; Linear Stretching sheet; Runge-Kutta method

1. INTRODUCTION

The fundamentals of nanofluids, slip effects, and their combined consequences in diverse applications are covered in this introduction. Slip at fluid-solid contacts introduces a distinctive boundary condition that substantially influences general flow characteristics. Concentration, thermal, and velocity slip are among the numerous types of slip effects in fluid dynamics that distinguish them from the typical no-slip situation at the solid-fluid interface. In-depth comprehension of the interactions between numerous slide effects and their impact on fluid flow is required as complexity increases. The flux of boundary layers is significantly influenced by thermal slip conditions, which has an impact on both industrial and natural processes. These processes encompass the extrusion of plastic and metal, as well as the refrigeration and drying processes employed in the production of paper and textiles. These characteristics have an impact on a variety of technical applications, including oil recovery, heat exchangers, catalytic reactors with rectangular ducts, chemical vapor deposition on surfaces, and chemical reactions in reactor chambers. Flow models in porous media are applicable in a variety of biological contexts, including brain tissue diffusion, tissue bio-heat transfer during genesis, blood flow in cancer, and bioconvection. Authors mentioned in the literature [1]-[5] developed a model that considers slip effects on time-dependent magnetohydrodynamic (MHD) heat and mass transfer through a porous stretching sheet. The model shows that slip parameter values increase and the fluid's velocity near the boundary layer region decreases. Other studies have focused on the multiple slip effects on MHD axisymmetric buoyant nanofluid flow above a stretching sheet, the presence of magnetic nanoparticles, the numerous slip effects on erratic viscoelastic nanofluid flow across a permeable stretched sheet with radiation, the thickness and velocity of the slip layer in

---

* Corresponding author: prof.murali20@gmail.com

concentrated suspensions, the influence of absorption and boundary slip in a channel, entropy analysis in a 3-D non-linear radiative hybrid nanofluid flow between two parallel stretched permeable sheets with slip velocities, and the Darcy-Forchheimer up/down flow of entropy optimized radiative nanofluids with second-order slip, nonuniform source/sink, and shape effects.Authors in the references section [6]-[10] et al. studied multiple slip and cross diffusion on MHD Carreau-Casson fluid over a slandering sheet with non-uniform heat source/sink. Asmat et al. examined thermal analysis in electrically conducting fluid with varying slips and radiation. Das et al. examined absorption and boundary slip in a channel. Nayak et al. investigated 3-D non-linear radiative hybrid nanofluid flow between two parallel stretched permeable sheets with slip velocities. Samantaray et al. studied Darcy-Forchheimer up/down flow of entropy optimized radiative nanofluids.

In geophysical systems and chemical engineering, cross-diffusion-that which results from instantaneous heat and mass transfer in a flowing fluid-is seen in the Soret and Dufour effects. Thermal diffusion-sometimes known as the Soret effect-describes specifically the mass transfer resulting from a temperature difference. The energy flow arising from changes in concentration is known as the Dufour effect. The Soret effect results from the separation of big, heavy molecules and small, light ones brought about by temperature differential. Many times, this effect is considered when many chemical species exist in a chemical environment with a notable temperature gradient. Many researchers drew interest in the Soret and Dufour effects on various fluid flow systems. references [11]-[15]cited in the section have studied steady free convective flow with Soret and Dufour effects using heat radiation and a magnetic field on porous materials. Shojaei et al. examined the Dufour and Soret effect in a convective stretchable cylinder, Hayat et al. studied the influence of Soret and Dufour effects on MHD Casson fluid flow, Pal and Mondal analyzed the impact of heat-generating and nonlinear thermal radiation on steady-state flow through a non-isothermal wedge, and Bekezhanova and Goncharova examined the properties of liquid flows undergoing evaporation. Authors mentioned in the references section [16]-[20]studied the impact of Soret and Dufour effects on forced convection flow towards a moveable thin needle using Buongiorno's nanofluid model. Jawad et al. analyzed boundary layer MHD Darcy-Forchheimer radiative nanofluid flow using Marangoni convection and also studied fluid flow dynamics in Soret-Dufour collisions. Das and Majumdar investigated the magnetohydrodynamic flow of a Casson fluid on an inclined permeable plate, considering the Soret effect, thermal radiation, viscous dissipation, and joule heating. Raja Sekhar et al. studied the movement of a magnetohydrodynamic Casson nanofluid across a non-linear inclined surface.The works mentioned in the literature [21]–[25] had a significant impact on understanding the nature of the reported work.Works which were done by the authors [27]-[32] have shown the solutions for the problems. The works mentioned in the literature [33]–[34] had a significant impact on understanding the nature of the reported work.

Motivated by the above research, this current research is a follow-up to the "MHD three-dimensional Casson fluid flow past a porous linearly stretching sheet" by Nadeem et al. [26]. The dynamics of the boundary layer of a nanofluid moving through a stretched sheet in a magnetic field is studied here by taking Multiple slips (Thermal and Concentration slips), Dufour and Soret effects into account. The set of regulating parameters determines how the governing equations are transformed into nonlinear differential equations. These non-linear differential equations are then numerically solved using the Runge-Kutta algorithm, along with shooting technique. a considerable physical quantity may be numerically calculated using tables, such as the local skin-friction coefficient, local Nusselt and Sherwood numbers, and so on. This non-linear stretching sheet has designs and structures that are ideal for the mechanical, aerospace, civil, and marine industries.

2. FLOW GOVERNING EQUATIONS

This work investigates the three-dimensional, continuously flowing, electrically conductive, non-compressible Casson-Nanofluid around a linearly stretched sheet. The work uses numerical techniques to identify answers while accounting for the effects of Soret, Dufour, porous media, multiple slips,

thermophoresis, and Brownian motion. The geometry and physical coordinate system of this flow problem are shown in Figure 1.
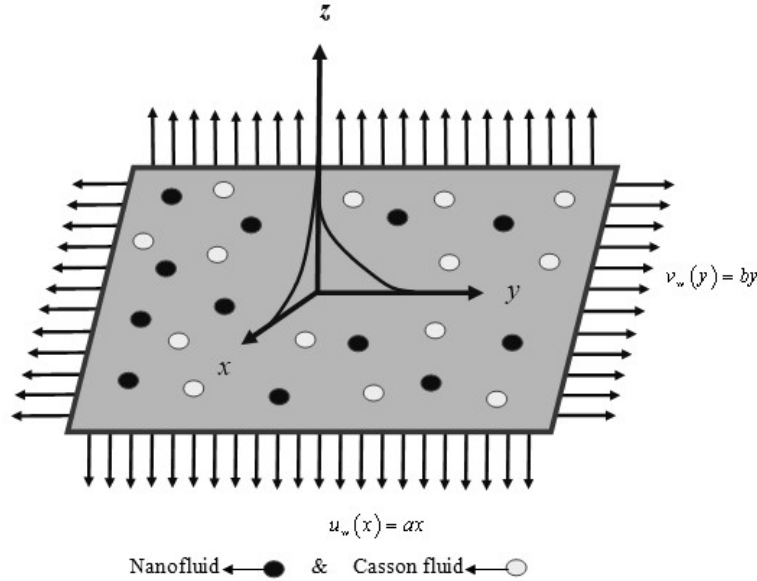

Fig. 1. Geometric representation of the movement of Casson and Nanofluid particles

a) Let (u, v, w) be the velocity components along the (x, y, z) directions, respectively.
b) Flow is generated due to an exponentially stretching surface.
c) A uniform magnetic field of strength B_0 is applied in the $z-$ direction.
d) Magnetic Reynolds number is assumed very small so that the induced magnetic field is ignored.
e) The effects of Soret and Dufour are considered in concentration and energy equations respectively.
f) The effects of multiple slip effects are considered in boundary conditions section.
g) The characteristics of Brownian motion and thermophoresis are accounted.
h) The rheological equation for a non-Newtonian fluid is defined as,

$$\tau = \tau_o + \mu \alpha^* \tag{1}$$

Eq. (1) can be expanded for Casson fluid as,

$$\tau_{ij} = \left\{ 2\left(\mu_B + \frac{p_y}{\sqrt{2\pi}} \right) e_{ij}, \ \pi > \pi_c \ \& \ 2\left(\mu_B + \frac{p_y}{\sqrt{2\pi_c}} \right) e_{ij}, \ \pi < \pi_c \right. \tag{2}$$

Where $\pi = e_{ij} e_{ji}$ with e_{ij} is the $(i, j)^{th}$ component of the fluid deformation rate and $p_y = \frac{\mu_B \sqrt{2\pi}}{\beta}$ is the yield stress of the Casson fluid.

For this flow, the governing boundary layer equations can be written as
Continuity Equation:

$$\frac{\partial u}{\partial x} + \frac{\partial v}{\partial y} + \frac{\partial w}{\partial z} = 0 \tag{3}$$

Momentum Equation:

$$u\left(\frac{\partial u}{\partial x} \right) + v\left(\frac{\partial u}{\partial y} \right) + w\left(\frac{\partial u}{\partial z} \right) = v\left(1 + \frac{1}{\beta} \right)\left(\frac{\partial^2 u}{\partial z^2} \right) - \left(\frac{v}{k^*} \right)u - \left(\frac{\sigma B_o^2}{\rho} \right)u \tag{4}$$

$$u\left(\frac{\partial v}{\partial x} \right) + v\left(\frac{\partial v}{\partial y} \right) + w\left(\frac{\partial v}{\partial z} \right) = v\left(1 + \frac{1}{\beta} \right)\left(\frac{\partial^2 v}{\partial z^2} \right) - \left(\frac{v}{k^*} \right)v - \left(\frac{\sigma B_o^2}{\rho} \right)v \tag{5}$$

Equation of thermal energy:

$$u\left(\frac{\partial T}{\partial x}\right)+v\left(\frac{\partial T}{\partial y}\right)+w\left(\frac{\partial T}{\partial z}\right)=\alpha\left(\frac{\partial^2 T}{\partial z^2}\right)+\tau_1\left\{D_B\left(\frac{\partial T}{\partial z}\right)\left(\frac{\partial C}{\partial z}\right)+\frac{D_T}{T_\infty}\left(\frac{\partial T}{\partial z}\right)^2\right\}+\frac{D_m K_T}{C_s C_p}\left(\frac{\partial^2 C}{\partial y^2}\right) \quad (6)$$

Equation of species concentration:

$$u\left(\frac{\partial C}{\partial x}\right)+v\left(\frac{\partial C}{\partial y}\right)+w\left(\frac{\partial C}{\partial z}\right)=D_B\left(\frac{\partial^2 C}{\partial z^2}\right)+\frac{D_T}{T_\infty}\left(\frac{\partial T}{\partial z}\right)^2+\frac{D_m K_T}{T_m}\left(\frac{\partial^2 T}{\partial y^2}\right) \quad (7)$$

The boundary conditions for this flow are

$$u=u_w(x)=ax,\; v=v_w(y)=by,\; T=T_w+L_1\left(\frac{\partial T}{\partial y}\right),\; C=C_w+L_2\left(\frac{\partial C}{\partial y}\right)\; at\; z=0 \left.\right\} \quad (8)$$

$$u\to 0,\; v\to 0,\; T\to T_\infty,\; C\to C_\infty\; as\; z\to\infty$$

Introducing the following similarity transformations

$$u=a(x+y)f'(\eta),\; v=b(x+y)g'(\eta),\; \phi=\frac{C-C_\infty}{C_w-C_\infty},$$
$$w=-\sqrt{av}\left\{f(\eta)+\Omega g(\eta)\right\},\; \eta=\left(\sqrt{\frac{a}{v}}\right)z,\; \theta=\frac{T-T_\infty}{T_w-T_\infty}, \left.\right\} \quad (9)$$

Making use of Eq. (9), equation of continuity is identically satisfied and Eqs. (4), (5), (6) and (7) take the following form

$$\left(1+\frac{1}{\beta}\right)f'''+ff''+gf''-f'^2-(M+K)f'=0 \quad (10)$$

$$\left(1+\frac{1}{\beta}\right)g'''+fg''+gg''-g'^2-(M+K)g'=0 \quad (11)$$

$$\theta''+\Pr f\theta'+\Pr g\theta'+\Pr Nb\theta'\phi'+\Pr Nt\theta'^2+\Pr Du\phi''=0 \quad (12)$$

$$Nb\phi''+NbScf\phi'+NbScg\phi'+Nt\theta''+ScNbSr\theta''=0 \quad (13)$$

the corresponding boundary conditions (8) become

$$f(0)=0,\; g(0)=0,\; f'(0)=1,\; g'(0)=\Omega,\; \theta(0)=1+\delta\theta'(0),\; \phi(0)=1+\lambda\phi'(0) \left.\right\} \quad (14)$$

$$f'(\infty)\to 0,\; g'(\infty)\to 0,\; \theta(\infty)\to 0,\; \phi(\infty)\to 0$$

where the involved physical parameters are defined as

$$M=\frac{\sigma B_o^2}{\rho a},\; Nb=\frac{\tau_1 D_B(C_w-C_\infty)}{v},\; Nt=\frac{v D_T(T_w-T_\infty)}{v T_\infty},$$
$$Sc=\frac{v}{D_B},\; K=\frac{1}{ak^*},\; Sr=\frac{D_m K_T(T_w-T_\infty)}{T_m v(C_w-C_\infty)},\; \delta=L_1\sqrt{\frac{a}{v}},$$
$$\Pr=\frac{v}{\alpha},\; Du=\frac{D_m K_T(C_w-C_\infty)}{C_s C_p v(T-T_\infty)},\; \lambda=L_2\sqrt{\frac{a}{v}},\; \Omega=\frac{b}{a}, \left.\right\} \quad (15)$$

Engineering quantities

Quantities of physical interest, the physical parameters of the skin-friction coefficient along x and y - directions and local Nusselt number are presented as follows:

$$Cf_x=\frac{\tau_{wx}}{\rho u_w^2}\Rightarrow\left(\sqrt{Re_x}\right)Cf_x=\left(1+\frac{1}{\beta}\right)f''(0) \quad (16)$$

$$Cf_y=\frac{\tau_{wy}}{\rho u_w^2}\Rightarrow\left(\sqrt{Re_y}\right)Cf_y=\left(1+\frac{1}{\beta}\right)g''(0) \quad (17)$$

$$Nu=\frac{xq_w}{\kappa(T_w-T_\infty)}=-\frac{x\left(\frac{\partial T}{\partial z}\right)_{z=0}}{\kappa(T_w-T_\infty)}\Rightarrow Nu=-\left(\sqrt{Re_x}\right)\theta'(0) \quad (18)$$

$$Sh = \frac{x q_m}{D_B\left(C_w - C_\infty\right)} = -\frac{x\left(\dfrac{\partial C}{\partial y}\right)_{y=0}}{D_B\left(C_w - C_\infty\right)} \Rightarrow Sh = -\left(\sqrt{\mathrm{Re}_x}\right)\phi'(0) \tag{19}$$

where $\mathrm{Re}_x = \dfrac{u_x(x)x}{\nu}$ is local Reynolds number based on the stretching velocity $u_w(x)$ and

$\mathrm{Re}_y = \dfrac{v_w(y)y}{\nu}$ is local Reynolds number based on the stretching velocity $v_w(y)$.

3. SOLUTION BY R-K METHOD ALONG WITH SHOOTING TECHNIQUE

Using the Runge-Kutta method alongside the shooting approach allows for the solution of non-linear governing equations with partial derivatives. This approach produces more accurate outcomes when compared to alternative numerical methods. Similarity transformations are employed to convert the controlling partial differential equations into ordinary differential equations. Through the use of additional variables, the non-linear equations are converted into linear equations. Introducing additional variables into a higher-order differential equation to convert it into a linear equation.

$$\left. f_1 = f,\ f_2 = f',\ f_3 = f'',\ f_4 = g,\ f_5 = g',\ f_6 = g'',\ f_7 = \theta,\ f_8 = \theta',\ f_9 = \phi,\ f_{10} = \phi' \right\} \tag{20}$$

The equations (13)-(15) are transformed to following first order ODE.

$$\left. \begin{aligned} f_3 &= f_2',\ f_3' = \frac{-f_1 f_3 - f_4 f_3 + f_2^2 + (M+K)f_2}{\left(1 + \dfrac{1}{\beta}\right)}, \\[2mm] f_6 &= f_5',\ f_6' = \frac{-f_1 f_6 - f_4 f_6 + f_5^2 - (M+K)f_5}{\left(1 + \dfrac{1}{\beta}\right)}, \\[2mm] f_8' &= -\Pr f_1 f_8 - \Pr f_4 f_8 - \Pr Nb f_8 f_{10} - \Pr Nt f_8^2 - \Pr Du\, f_{10}', \\[2mm] f_{10}' &= \frac{-Nb\, Sc f_1 f_{10} - NbSc f_4 f_{10} - Nt\, f_8' - ScNbSr f_8'}{Nb} \end{aligned} \right\} \tag{21}$$

Using Eq. (21), the corresponding boundary conditions (16) are

$$\left. \begin{aligned} &f_1(0) = 0,\ f_4(0) = 0,\ f_2(0) = 1,\ f_5(0) = \Omega,\ f_7(0) = 1 + \delta f_8(0),\ f_9(0) = 1 + \lambda f_{10}(0) \\ &f_2(\infty) \to 0,\ f_5(\infty) \to 0,\ f_7(\infty) \to 0,\ f_9(\infty) \to 0 \end{aligned} \right\} \tag{22}$$

The approximate solutions are numerically resulted in graphical representation using MATLAB bvp4c programming to present the physical significance of non-dimensional parameters. The iterative procedure is repetitive till we obtained results correct up to the preferred precision of 10^{-6} level.

3.1. Comparison of Present Results with Published Results

Table 1 Valuation of present Skin-friction results with published results
of Nadeem et al. [26] when $Sr = Nb = \text{Pr} = Sc = Nt = Du = \lambda = \delta = 0$, and $\beta \to \infty$.

M	Present $\left(1+\dfrac{1}{\beta}\right)f''(0)$ results		Nadeem et al. [21] $\left(1+\dfrac{1}{\beta}\right)f''(0)$ results		Present $\left(1+\dfrac{1}{\beta}\right)g''(0)$ results	
	$\Omega = 0.0$	$\Omega = 0.5$	$\Omega = 0.0$	$\Omega = 0.5$	$\Omega = 0.5$	$\Omega = 1.0$
0.0	1.7288585	1.8275432	1.7320	1.8361	0.8145634	1.9245632
10.0	4.7852352	4.8256702	4.7958	4.8310	2.3758347	4.8535761

For comparison of present results with the published results, the authors have compared the present Skin-friction results with published results of Nadeem et al. [26] for variations of M at $\beta \to \infty$ in Table 1 when $Sr = Nb = \text{Pr} = Sc = Nt = Du = \lambda = \delta = 0$. This table exposes a good agreement between the current findings and those obtained by Nadeem et al. [26], as previously stated.

4. RESULTS AND DISCUSSION

On a Casson-nanofluid stream over a linearly stretching sheet, an analysis of three-dimensional, steady flow was performed. Due to the combination of Soret and Dufour, an electrically charged fluid is investigated in the presence of Magnetic field and Multiple slip effects. An approximate numerical approach called Runge Kutta method along with shooting technique is used to handle the altered equations created from the said model. Examine the effects of various dynamic parameters of the contours of our system on velocity, and temperature, and concentration profiles. Also, the study of variables for different values through the graphs. For this study, we have taken on the settings of engineering parameters for our study as $M = 0.5$, $K = 0.3$, $\beta = 0.5$, $\text{Pr} = 0.71$, $Nb = 0.3$, $Nt = 0.5$, $Du = 0.5$, $Sc = 0.22$, $Sr = 0.5$, $\Omega = 0.5$, $\delta = 0.5$, and $\lambda = 0.5$.

The figures, 2 and 3, clearly demonstrate that when the magnetic field parameter increases, both the boundary layer thickness and the amplitude of the main and secondary velocity profiles decrease. Physically, the current phenomenon occurs when a magnetic field causes the flow of electric current in a conductive fluid. This results in the fluid inside the boundary layer encountering a drag force, which decelerates the fluid's velocity. Therefore, the use of magnetic fields is terminated.

The figures 4 and 5 demonstrate that the primary and secondary velocity profiles inside the boundary layer diminish as the porosity parameter rises. In addition, Figures 4 and 5 illustrate that an increase in the permeability parameter leads to a reduction in the thickness of the boundary layer.

The influence of the non-Newtonian Casson fluid parameter on the primary and secondary velocity profiles may be seen in Figures 6 and 7. It is shown that the resistance to the flow of fluid is caused by an elevation in the non-Newtonian Casson fluid parameter. In Figures 6 and 7, it can be shown that when the non-Newtonian Casson fluid parameter has bigger values, the amplitude of the main and secondary velocity profiles, as well as the thickness of the boundary layer, decrease. It is observed that when we increase the non-Newtonian Casson fluid parameter indefinitely, the present events obviously transition to a Newtonian fluid.

Figure 8 illustrates the impact of the Stretching ratio parameter on the secondary velocity profiles. The secondary velocity profiles increase as the value of the stretching rate ratio parameter grows. Generally, increasing the stretching parameter leads to a rise in flow pressure. The fluid's temperature in relation to the Prandtl number is shown in Figure 9. As the Prandtl number increases, the temperature differential in the fluid decreases. Lower thermal diffusivity in fluids with a higher Prandtl number results in a lower temperature.

The temperature and the concentration profiles are both influenced by the Brownian motion parameter, as Figures 10 and 11 respectively demonstrate. Figure 10 illustrates how increasing the Brownian motion parameter results in improved temperature profiles. As the viscous force decreases and the Brownian motion parameter increases, the Brownian diffusion coefficient increases. As a result, both temperature and the thermal boundary layer's thickness vary. These effects might be better understood by looking at Figure 10. It is evident from Figure 11 that as the Brownian motion parameter increases, the concentration falls. The impact of the thermophoresis parameter on the temperature and concentration curves is seen in Figures 12 and 13, respectively. The thermophoresis parameter is defined by the viscous force and the heat diffusion coefficient. As its inversely proportional nature implies, a decrease in the viscous force occurs with an increase in the thermophoresis parameter. The thermophoresis value indicates that the temperature and nanoparticle concentration have increased due to a decrease in viscous force and an increase in the thermal diffusion coefficient.

Figure 14 illustrates how the fluid's temperature profile rises as the number of Dufour increases. This phenomenon may be explained by describing the release of two chemically insensitive fluids at room temperature inside a system, which increases the system's internal temperature differential. Figure 15 shows how the number of Soret affects concentration profiles, indicating that an increase in Soret number results in an increase in liquid concentration. The Soret effect occurs when an irreversible process generates a temperature gradient in a concentration field. It has the ability to increase the circulatory system's concentration flow. The original reason is shown in Figure 15.

In Figure 16, you can see how the thermal slip measure changes the temperature curve. As the slip limit gets bigger, the temperature goes down. When the thermal slip parameter goes up, the thickness of the thermal boundary layer goes down, even though there isn't much heat transfer from the layer to the fluid. As the concentration slip parameter goes up, the concentration curve goes down, as shown in Figure 17.

Figure 18 illustrates the impact of Schmidt number on concentration patterns. The Schmidt number is a dimensionless quantity that denotes the ratio of momentum to mass diffusivity. By diffusion in the concentration (species) boundary layer, the comparative magnitudes of momentum and mass transfer are determined by the calculation. The concentration will decrease as a result of the fluid's lower mass diffusivity, which is a consequence of a higher Schmidt number. The Schmidt number and mass diffusivity are inversely proportional, indicating that concentration boundary layers with higher Schmidt numbers are thinner.
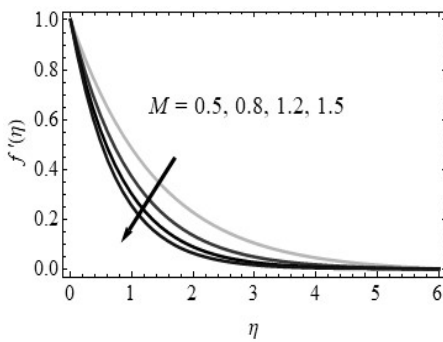

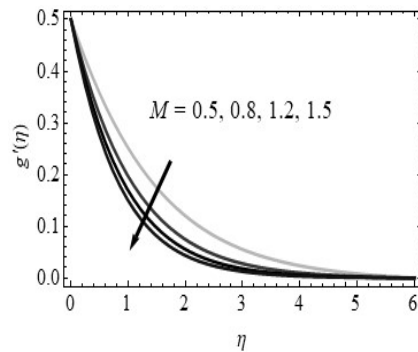**Fig. 2.** Influence of M on $f'(\eta)$ velocity profiles

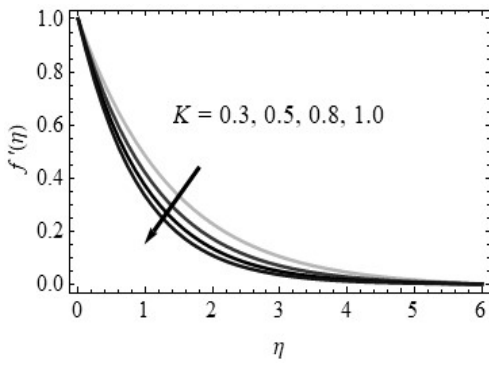**Fig. 3.** Influence of M on $g'(\eta)$ velocity profiles

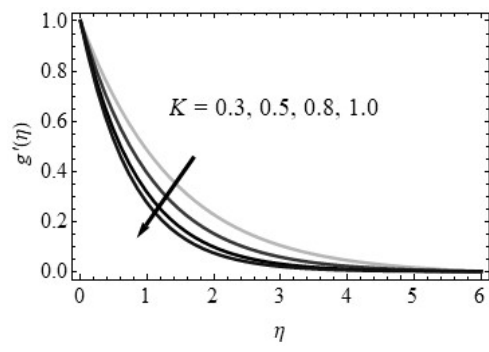**Fig. 4.** Influence of K on $f'(\eta)$ velocity profiles

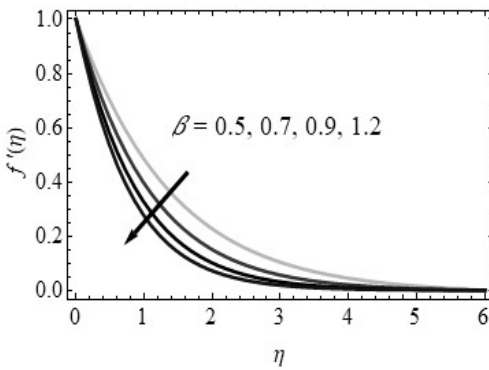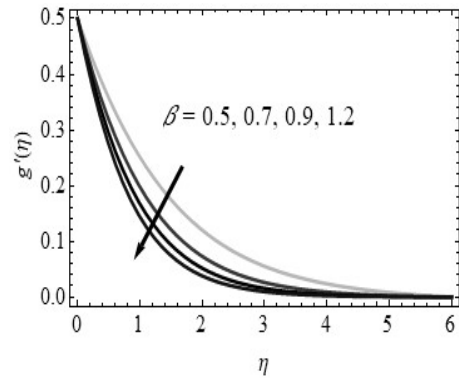**Fig. 5.** Influence of K on $g'(\eta)$ velocity profiles

Fig. 6. Influence of β on $f'(\eta)$ velocity profiles

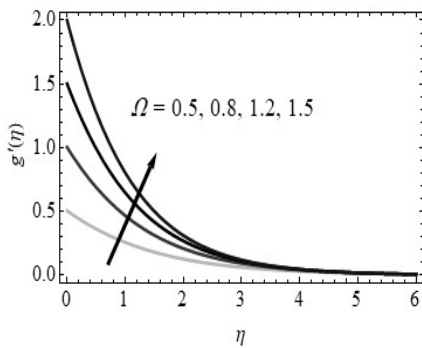**Fig. 7.** Influence of β on $g'(\eta)$ velocity profiles

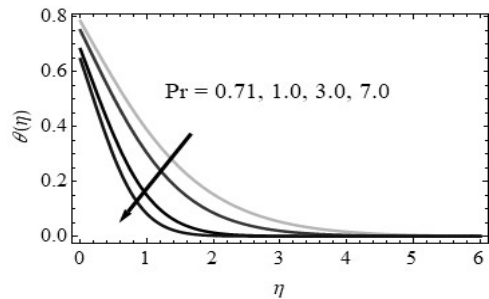**Fig. 8.** Influence of Ω on $g'(\eta)$ velocity profiles

Fig. 9. Influence of Pr on $\theta(\eta)$ temperature profiles

Fig. 10. Influence of Nb on $\theta(\eta)$ temperature profiles

Fig. 11. Influence of Nb on $\phi(\eta)$ concentration profiles

Fig. 12. Influence of Nt on $\theta(\eta)$ temperature profiles

Fig. 13. Influence of Nt on $\phi(\eta)$ concentration profiles
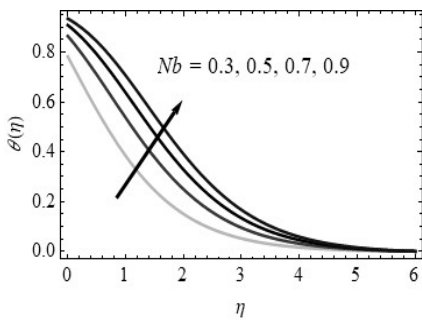

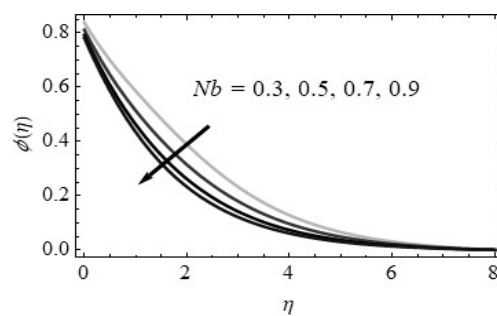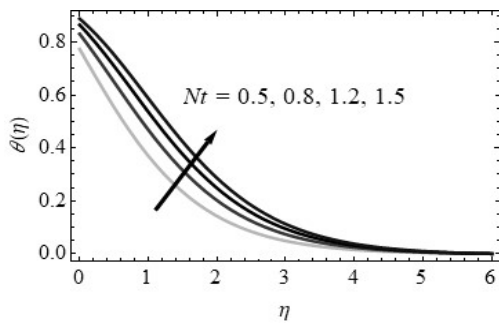**Fig. 14.** Influence of Du on $\theta(\eta)$ temperature profiles

Fig. 15. Influence of Sr on $\phi(\eta)$ concentration profiles

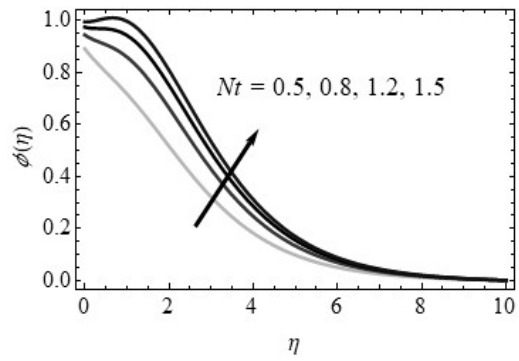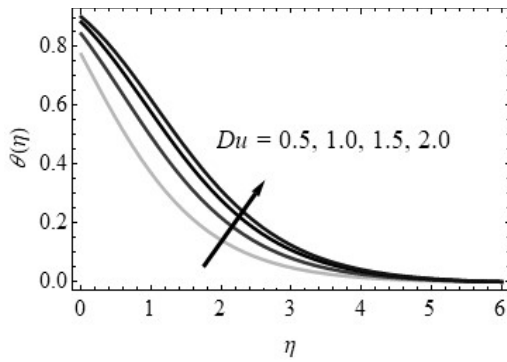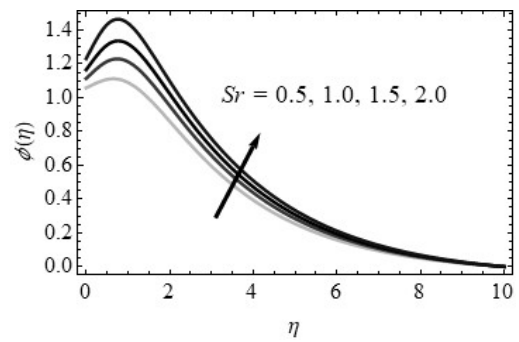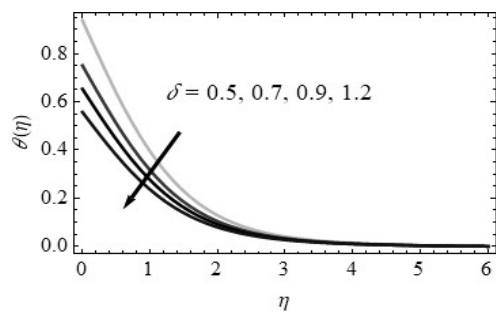**Fig. 16.** Influence of δ on $\theta(\eta)$ temperature profiles
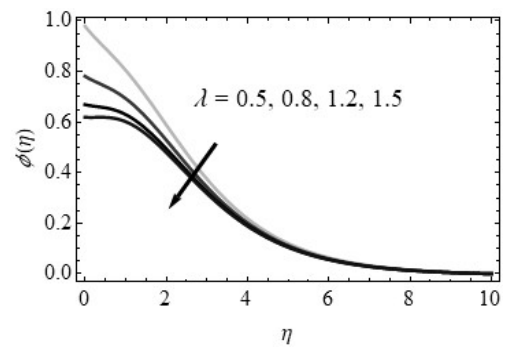

Fig. 17. Influence of λ on $\phi(\eta)$ concentration profiles
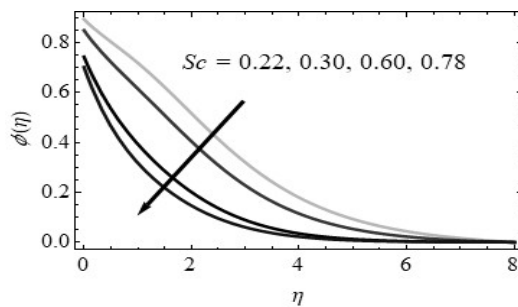

Fig. 18. Influence of Sc on $\phi(\eta)$ concentration profiles

Table 2 Skin-friction coefficient $\left(1+\dfrac{1}{\beta}\right)f''(0)$ numerical values

M	K	β	Ω	Pr	Nb	Nt	Du	δ	Sc	Sr	λ	$\left(1+\dfrac{1}{\beta}\right)f''(0)$
0.5	0.3	0.5	0.5	0.71	0.3	0.5	0.5	0.5	0.22	0.5	0.5	1.8563629652
0.8												1.8158282823
1.2												1.7956738784
	0.5											1.8067859839
	0.8											1.7842383084
		0.7										1.8256764870
		0.9										1.7934574573
			0.8									1.8858288221
			1.2									1.9168756287
				1.00								1.8067762857
				3.00								1.7745654726
					0.5							1.8945652975
					0.7							1.9245629259
						0.8						1.9035482582
						1.2						1.9354665928
							1.0					1.9156760876
							1.5					1.9565876878
								0.7				1.8257106508
								0.9				1.8065865818
									0.30			1.8046496591
									0.78			1.7945635972
										1.0		1.8846658658
										1.5		1.9354345082
											0.8	1.8258582830
											1.2	1.8067730304

The effects of Thermophoresis parameter (Nt = 0.5, 0.8, 1.2), Brownian motion parameter (Nb = 0.3, 0.5, 0.7), Soret number (Sr = 0.5, 1.0, 1.5), Concentration slip parameter (λ = 0.5, 0.8, 1.2), and Schmidt number (Sc = 0.22, 0.30, 0.60). on rate of mass transfer coefficient or in terms Sherwood number coefficient are discussed in Table-4. From this table, it is observed that the rate of mass transfer coefficient is increasing with increasing values of Thermophoresis parameter (Nt = 0.5, 0.8, 1.2) and decreasing with increasing values of Brownian motion parameter (Nb = 0.3, 0.5, 0.7), Soret number (Sr = 0.5, 1.0, 1.5), Concentration slip parameter (λ = 0.5, 0.8, 1.2), and Schmidt number (Sc = 0.22, 0.30, 0.60).

Table 2 shows the numerical values of Skin-friction coefficient due to primary velocity profiles for variations in values of the engineering parameters such as, Magnetic field parameter (M = 0.5, 0.8, 1.2), Permeability parameter (K = 0.3, 0.5, 0.8), Casson fluid parameter (β = 0.5, 0.7, 0.9), Prandtl number (Pr = 0.71, 1.0, 3.0), Thermophoresis parameter (Nt = 0.5, 0.8, 1.2), Brownian motion parameter (Nb = 0.3, 0.5, 0.7), Dufour number (Du = 0.5, 1.0, 1.5), Soret number (Sr = 0.5, 1.0, 1.5), Thermal slip parameter (δ = 0.5, 0.7, 0.9), Concentration slip parameter (λ = 0.5, 0.8, 1.2), Stretching sheet parameter (Ω = 0.5, 0.8, 1.2) and Schmidt number (Sc = 0.22, 0.30, 0.60). From this table, it is observed that the Skin-friction coefficient is increasing with rising values of Stretching sheet parameter (Ω = 0.5, 0.8, 1.2), Thermophoresis parameter (Nt = 0.5, 0.8, 1.2), Brownian motion parameter (Nb = 0.3, 0.5, 0.7), Dufour number (Du = 0.5, 1.0, 1.5), Soret number (Sr = 0.5, 1.0, 1.5), while it is decreasing with increasing values of Magnetic field parameter (M = 0.5, 0.8, 1.2), Permeability parameter (K = 0.3, 0.5, 0.8), Casson fluid parameter(β = 0.5, 0.7, 0.9), Prandtl number (Pr=0.71,1.0,3.0),Thermal slip parameter (δ = 0.5, 0.7, 0.9),Concentration slip parameter(λ = 0.5, 0.8, 1.2), and Schmidt number (Sc = 0.22, 0.30, 0.60).

Table-3.: Skin-friction coefficient $\left(1+\dfrac{1}{\beta}\right)g''(0)$ numerical values

M	K	β	Ω	Pr	Nb	Nt	Du	δ	Sc	Sr	λ	$\left(1+\dfrac{1}{\beta}\right)g''(0)$
0.5	0.3	0.5	0.5	0.71	0.3	0.5	0.5	0.5	0.22	0.5	0.5	0.4366750857
0.8												0.3965760101
1.2												0.3656671086
	0.5											0.4167403701
	0.8											0.3856750385
		0.7										0.4067685989
		0.9										0.3746502354
			0.8									0.4645462482
			1.2									0.4845881772
				1.00								0.3976868198
				3.00								0.3567777081
					0.5							0.4756165023
					0.7							0.5056650185
						0.8						0.4806547108
						1.2						0.5141769232
							1.0					0.4967603643
							1.5					0.5256897128
								0.7				0.4067832591
								0.9				0.3856740633
									0.30			0.4063634014
									0.78			0.3677461449
										1.0		0.4612576708
										1.5		0.5034906340
											0.8	0.3965760137
											1.2	0.3518576825

The numerical values of rate of heat transfer coefficient in terms of Nusselt number are displayed in table-3 for different values of Prandtl number (Pr = 0.71, 1.0, 3.0), Thermophoresis parameter *(Nt = 0.5, 0.8, 1.2)*, Brownian motion parameter *(Nb = 0.3, 0.5, 0.7)*, Dufour number *(Du = 0.5, 1.0, 1.5)*, and Thermal slip parameter *(δ = 0.5, 0.7, 0.9)*. From this table, it is observed that the rate of heat transfer coefficient is gradually rising with increasing values of Thermophoresis parameter *(Nt = 0.5, 0.8, 1.2)*, Brownian motion parameter *(Nb = 0.3, 0.5, 0.7)*, Dufour number *(Du = 0.5, 1.0, 1.5)*, while the reverse effect is observed in increasing values of Prandtl Number (Pr = 0.71, 1.0, 3.0) and Thermal slip parameter *(δ = 0.5, 0.7, 0.9)*.

Table-4.: Rate of heat transfer coefficient $-\theta'(0)$ numerical values

Pr	Nb	Nt	Du	δ	$-\theta'(0)$
0.71	0.3	0.5	0.5	0.5	0.8755277123
1.00					0.8356746803
3.00					0.8015465292
	0.5				0.9056751045
	0.7				0.9354859826
		0.8			0.9105965752
		1.2			0.9456756037
			1.0		0.9216576501
			1.5		0.9454658522
				0.7	0.8465710456
				0.9	0.8216587815

Table-5.: Rate of mass transfer coefficient $-\phi'(0)$ numerical values

Nb	Nt	Sc	Sr	λ	$-\phi'(0)$
0.3	0.5	0.22	0.5	0.5	0.9156736034
0.5					0.8719546129
0.7					0.8356761852
	0.8				0.9365781087
	1.2				0.9512539732
		0.30			0.8656708544
		0.78			0.8154043804
			1.0		0.9367165760
			1.5		0.9554598181
				0.8	0.8845881953
				1.2	0.8656746818

5. CONCLUSIONS

In the current research work, the joint effects of Soret and Dufour, Brownian motion on three-dimensional, steady, incompressible, electrically conducting, viscous, Casson-Nanofluid flow towards a stretching sheet in presence of porous medium, magnetic field and Multiple slip effects is investigated. For this investigation, the resultant governing flow equations are solved by using Runge-Kutta method along with shooting technique. The aspire of this research article is to examine the impacts of $M, \beta, K, \Omega, Du, Sr, \Pr, \delta, Sc, Nb, Nt, \lambda$ on flow variables such as velocity, temperature, and concentration profiles as well as Skin-friction, rate of heat and mass transfer coefficients are studied through graphically and tabular forms. From this investigation, the main findings are:

- An increase in the parameters of the magnetic field, Casson fluid, and porous material leads to a decrease in the main velocity profiles.
- As the Stretching sheet parameter grows, the secondary velocity profiles similarly increase. However, the magnetic field, Casson fluid, and porous medium parameters exhibit the reverse tendency.
- The temperature profile of the nanofluid demonstrates enhanced performance when the thermophoresis, Dufour effect, and Brownian motion are increased. Furthermore, it exhibits a diminishing trend when the Prandtl number and thermal slip parameter are large.
- The concentration profiles drop as the Schmidt number, concentration slip parameter, and Brownian motion parameters increase, and increase as the thermophoresis and Soret parameters increase.
- By using a constraining scenario, the numerical results obtained are ultimately more precise in comparison to the published findings of Nadeem et al. [26] for $Sr = Nb = \Pr = Sc = Nt = Du = \lambda = \delta = 0$, and $\beta \rightarrow \infty$.

REFERENCES

[1] Asmat, F., Khan, W. A., Shamshuddin, M. D., Salawu, S. O. & Bouye, M. (2023). Thermal analysis in an electrically conducting fluid with multiple slips and radiation along a plate: a case study of Stokes' second problem, *Case Stud. Therm. Eng.*, **44**, 102831.

[2] Babu, N. V. N., Paul, A. & Murali, G. (2015). Soret and Dufour effects on unsteady hydromagnetic free convective fluid flow past an infinite vertical porous plate in the presence of chemical reaction, *Journal of science and arts*, **15**(1), 99–111.

[3] Babu, N. V. N., Murali, G. & Bhati, S. M. (2018). Casson fluid performance on natural convective dissipative couette flow past an infinite vertically inclined plate filled in porous medium with heat transfer, MHD and hall current effects, *International journal of Pharmaceutical Research,* **10**(4).

[4] Bekezhanova, V. B. & Goncharova, O. N. (2020). Influence of the Dufour and Soret effects on the characteristics of evaporating liquid flows, *Int. J. Heat Mass Tran.*, **154**, 119696.

[5]   Das, U. J. & Majumdar, N. M. (2024). Magnetohydrodynamic flow of Casson fluid on an inclined permeable moving plate with viscous dissipation, thermal radiation, Joule heating and Soret effect, *Latin American Applied Research*, **54**(4), 497–505.

[6]   Das, D., Shaw, S., Mondal, K. K. & Kairi, R. R. (2013). Analyzing the impact of boundary slip and absorption effects on the dispersion of solute in a pulsatile channel flow of Casson fluid under magnetic field, *Eur. Phys. J. Plus*, **138**(5), 372.

[7]   Deepa, G. & Murali, G. (2014). Effects of viscous dissipation on unsteady MHD free convective flow with thermophoresis past a radiate inclined permeable plate, *Iranian Journal of Science and Technology (Sciences)*, 38A3, doi: 10.22099/IJSTS.2014.2437

[8]   Eleni, S., Haile, E. & Walelign, T. (2022). Multiple slips, Soret and Dufour effects in fluid flow near a vertical stretching sheet in the presence of magnetic nanoparticles, *International Journal of Thermofluids*, **13**, 100136.

[9]   Gundagani, M., Sheri, S., Paul, A. & Reddy, M. C. K. (2013). Radiation Effects on an Unsteady MHD Convective Flow Past a Semi-Infinite Vertical Permeable Moving Plate Embedded in a Porous Medium with Viscous Dissipation, *Walailak J Sci & Tech*, **10**(5), 499–515.

[10] Gundagani, M., Babu, N. V. N., Gadially, D. et al. (2024). Study of Nano-Powell-Erying fluid flow past a porous stretching sheet by the effects of MHD, thermal and mass convective boundary conditions, *J. Umm Al-Qura Univ. Eng. Archit.*, doi: 10.1007/s43995-024-00056-2.

[11] Gundagani, M., Mamidi, L. P. & Tanuku, P. K. (2024). Finite element solutions of Double diffusion effects on three-dimensional MHD Nano-Powell-Erying fluid flow in presence of thermal and mass Biot numbers, *J. Eng. Appl. Sci.*, **71**(9), doi: 10.1186/s44147-023-00347-w.

[12] Gadipally, D. & Murali, G. (2014). Analysis of Soret and Dufour effects onunsteady MHD flow past a semi infinite vertical porous plate via finite difference method, *International journal of applied physics and mathematics*, **4**(5), 332–344, doi: 10.7763/IJAPM.2014.V4.306.

[13] Hayat, T., Shehzad, S. A. & Alsaedi, A. (2012). Soret and Dufour effects on magnetohydrodynamic (MHD) flow of Casson fluid, *Appl. Math. Mech.*, **33**, 1301–1312.

[14] Idowu, A. S. & Falodun, B. O. (2018). Influence of magnetic field and thermal radiation on steady free convective flow in a porous medium, *Nigerian J. Technol. Dev*, **15**(3), 84–97.

[15] Jawad, M., Saeed, A., Kumam, P., Shah, Z. & Khan, A. (2021). Analysis of boundary layer MHD Darcy-Forchheimer radiative nanofluid flow with Soret and Dufour effects by means of marangoni convection, *Case Stud. Therm. Eng.*, **23**, 100792.

[16] Kahn, S. A., Nie, Y., Ali & B. (2019). Multiple Slip Effects on Magnetohydrodynamic Axisymmetric Buoyant Nanofluid Flow above a Stretching Sheet with Radiation and Chemical Reaction, *Symmetry*, **11**(9), 1171, doi: 10.3390/sym11091171.

[17] Khan, S. A., Nie, Y. & Ali, B. (2020). Multiple slip effects on MHD unsteady viscoelastic nanofluid flow over a permeable stretching sheet with radiation using the finite element method, *SN Appl. Sci.,* **2**, 66, doi: 10.1007/s42452-019-1831-3.

[18] Mabood. F, & Stanford, S. (2019). Multiple slip effects on MHD unsteady flow heat and mass transfer impinging on a permeable stretching sheet with radiation, *Modelling and Simulation in Engineering*, **2019**(1), 1–11.

[19] Murali, G., Reddy, M. C. K. & Sivaiah, S. (2012). Finite element solution of thermal radiation effect on unsteady MHD flow past a vertical porous plate with variable suction, *American Academic & Scholarly Research Journal*, **4**(3), 3–22.

[20] Murali, G., Paul, A. & Babu, N. V. N. (2015). Numerical study of chemical reaction effects on unsteady MHD fluid flow past an infinite vertical plate embedded in a porous medium with variable suction, *Electronic Journal of mathematical analysis and applications*, **3**(2), 179–192

[21] Murali, G., Sivaiah, S., Paul, A. & Reddy, M. C. K. (2013). Unsteady magnetohydrodynamic free convective flow past a vertical porous plate, *International journal of applied science and engineering*, **11**(3), 267–275.

[22] Murali, G., Deepa, G., Kasturi, V. N. & Poornakantha, T. (2023). Joint effects of thermal diffusion and diffusion thermo on MHD three dimensional nanofluid flow towards a stretching sheet, *Mathematical models in engineering*, **9**(4), doi: 10.21595/mme.2023.23590.

[23] Murali, G. & Babu, N. V. N. (2023). Convective MHD Jeffrey Fluid Flow Due to Vertical Plates with Pulsed Fluid Suction: A Numerical Study, *Journal of computational applied mechanics*, doi: 10.22059/JCAMECH.2023.351326.773.

[24] Murali, G. & Babu, N. V. N. (2012). Effect of Radiation on MHD Convection Flow Past a Vertical Permeable Moving Plate, *International Journal of Advances in Applied Sciences*, **1**(1), 19–28.

[25] Murali, G., Paul, A. & Babu, N. V. N. (2015). Heat and mass transfer effects on an unsteady hydromagnetic free convective flow over an infinite vertical plate embedded in a porous medium with heat absorption, *Int. J. Open Problems Compt. Math*, **8**(1).

[26] Nadeem, S., Haq, R. U., Akbar, N. S. & Khan, Z. H. (2013). MHD three-dimensional Casson fluid flow past a porous linearly stretching sheet, *Alexandria Eng. J.*, **52**, 577–582.

[27] Nayak, M. K., Mahanta, G., Das, M. & Shaw, S. (2022). Entropy analysis of a 3D nonlinear radiative hybrid nanofluid flow between two parallel stretching permeable sheets with slip velocities, *Int. J. Ambient Energy*, **43**(1), 8710–8721.

[28] Pal, D. & Mondal, H. (2013). Influence of thermophoresis and Soret-Dufour on magnetohydrodynamic heat and mass transfer over a non-isothermal wedge with thermal radiation and Ohmic dissipation, *J. Magn. Magn. Mater.*, **331**, 250–255.

[29] Raju, C. S. K., Priyadarshini, P. & Ibrahim, S. M. (2017). Multiple Slip and Cross Diffusion on MHD Carreau-Casson fluid over a Slandering Sheet with Non-uniform Heat Source/Sink, *International Journal of Applied and Computational Mathematics,* **3**, 203–224.

[30] Salleh, S. N. A., Bachok, N., Arifin, N. M. & Ali, F. M. (2020). Influence of Soret and Dufour on forced convection flow towards a moving thin needle considering Buongiorno's nanofluid model, *Alex Eng. J.*, **59**(5), 3897–3906.

[31] Sekhar, P. R., Sreedhar, S., Ibrahim, S. M. & Kumar, P. V. (2023). Radiative Heat Source Fluid Flow of MHD Casson Nanofluid over A Non-Linear Inclined Surface with Soret and Dufour Effects, *CFD Letters*, **15**(7), 42–60, doi: 10.37934/cfdl.15.7.4260

[32] Shehzad, S. A., Abbas, Z., Rauf, A. & Abdelmalek, Z. (2021). Dynamics of fluid flow through Soret-Dufour impacts subject to upward and downward motion of rotating disk, *Int. Commun. Heat Mass*, **120**, 105025.

[33] Shojaei, A., Amiri, A. J., Ardahaie, S. S., Hosseinzadeh, K. & Ganji, D. D. (2019). Hydrothermal analysis of Non-Newtonian second-grade fluid flow on a radiative stretching cylinder with Soret and Dufour effects, *Case Stud. Thermal Eng*, **13**, 100384.

[34] Soltani, F. & Yilmazer, L. (2010). Slip velocity and slip layer thickness in flow of concentrated suspensions, *Appl. Polym. Sci.*, **70**, 515–522.